# Benchmarking DFT functionals for excited-state calculations of Donor Acceptor TADF emitters: Insights on the key parameters determining Reverse Inter System Crossing

*David Hall, [a, b] Juan Carlos Sancho-García,[c] Anton Pershin,[d] David Beljonne,[b] Eli Zysman-Colman[a]* and Yoann Olivier[e]**

Organic Semiconductor Centre, EaStCHEM School of Chemistry, University of St Andrews, St Andrews, UK, KY16 9ST. E-mail: eli.zysman-colman@st-andrews.ac.uk; http://www.zysman-colman.com

[b]Laboratory for Chemistry of Novel Materials, University of Mons, 7000, Mons, Belgium.

[c]Department of Physical Chemistry, University of Alicante, E-03080, Alicante, Spain;

[d]Wigner Research Centre for Physics, PO Box 49, Budapest, Hungary;

[e]Laboratory for Computational Modeling of Functional Materials, Namur Institute of Structured Matter, University of Namur, Rue de Bruxelles, 61, 5000 Namur, Belgium. E-mail: yoann.olivier@unamur.be

## Abstract

The importance of intermediate triplet states and the nature of excited states has gained interest in recent years for the thermally activated delayed fluorescence (TADF) mechanism. It is widely accepted that simple conversion between charge transfer (CT) triplet and singlet excited states is too crude, and a more complex route involving higher-lying locally excited triplet excited states has to be invoked to witness the magnitude of the rate of reverse intersystem crossing (RISC) rates. The increased complexity has challenged the reliability of computational

methods to accurately predict the relative energy between excited states as well as their nature. Here we compare the results of widely used DFT functionals, CAM-B3LYP, LC-ωPBE, LC-ω*PBE, LC-ω*HPBE, B3LYP, PBE0 and M06-2X against a wavefunction-based reference method, Spin-Component Scaling second-order approximate Coupled-Cluster (SCS-CC2) in fourteen known TADF emitters possessing a diversity of chemical structures. Overall, the use of the Tamm-Dancoff Approximation (TDA) together with the CAM-B3LYP, M06-2X and the two ω-tuned range-separated functionals LC-ω*PBE and LC-ω*HPBE demonstrated the best agreement with SCS-CC2 calculations in predicting the absolute energy of the singlet $S_1$, and triplet $T_1$ and $T_2$ excited states and their energy differences. However, consistently across the series and irrespective of the functional or the use of TDA, the nature of $T_1$ and $T_2$ is not as accurately captured as compared to $S_1$. The presented work highlights that despite good agreement of energies, the description of the exact nature of the triplet states should be undertaken with caution.

## 1) Introduction

Research focusing on materials that display thermally activated delayed fluorescence (TADF) has become very important in recent years due largely to their strong potential as emitters in electroluminescent devices, as imaging reagents in biological systems and as photocatalysts.[1-4] Although the photophysical concept of TADF has been known for decades,[5-8] it has only recently been recognized as a triplet harvesting pathway in organic light-emitting diodes (OLEDs).[9, 10] Spin statistics dictate that upon recombination of a hole and an electron, excitons will form in a 3:1 ratio of triplets to singlets.[2] Through TADF, an Internal Quantum Efficiency (IQE) of up to 100% is possible, matching the IQE of phosphorescent OLEDs.

In the TADF mechanism, the normally non-emissive triplet excitons are converted to emissive singlet through an endothermic reverse intersystem crossing (RISC). Intersystem crossing

(ISC) and RISC are formally spin-forbidden processes and are only possible when there is mixing of the $S_1$ to $T_1$ wavefunctions, which can be quantified in terms of the first-order mixing coefficient, λ, (equation 1).[11] This term is itself dependent on the degree of SOC between the singlet and triplet states and the energy difference between them, $\Delta E_{ST}$ (Eq. 1),

$$\lambda = \frac{SOC}{\Delta E_{ST}} \qquad (1)$$

SOC itself can only occur when the orbital type of the singlet and triplet states are distinct, thereby satisfying El Sayed's rules.[12] In D-A TADF materials, SOC between CT states of different spin multiplicities is forbidden while SOC between a CT state and a locally excited states (LE) is large (Figure ***1***). SOC is proportional to $Z^4$ (where Z is the atomic number) of the atoms involved in the transitions to $S_1$ and $T_1$.[13] This is the origin of the very fast ISC rates in phosphorescent metal complexes (usually iridium) and is coined the heavy atom effect. However, SOC is expected to be low in TADF emitters which are composed primarily of 1$^{st}$ and 2$^{nd}$ row elements. Decrease in $\Delta E_{ST}$ is facilitated by decoupling of the hole and the electron densities associated with $T_1$ and $S_1$ states, which occurs in CT states as opposed to LE states, which have strongly overlapping ground and excited state densities (Figure ***1*****b**).

Equation 1 characterizes the degree of state mixing between $T_1$ and $S_1$, which should be large to trigger efficient direct RISC from $T_1$ to $S_1$. However, a direct conversion from $T_1$ to $S_1$ is not necessarily the most efficient conversion path when the nature of $T_1$ and $S_1$ are largely similar as this results in a very small SOC. A spin vibronic mechanism can be invoked, where vibronic coupling between $T_1$ and higher lying triplet states ($T_n$) occurs, permitting reverse internal conversion (RIC) prior to RISC from the higher-lying $T_n$ state.[14] When the higher-lying triplet state is of different orbital type to $S_1$ (i.e., LE) then El Sayed's rules are satisfied, leading to non-negligible SOC and a large degree state mixing. Indeed, this mechanism is frequently invoked in the literature to explain fast $k_{RISC}$ rates despite the moderately large $\Delta E_{ST}$. Quantum

chemical calculations are frequently employed to rationalize such a mechanism by computing the higher-lying triplet excited states where spectral assignment is rather challenging.[15-19]

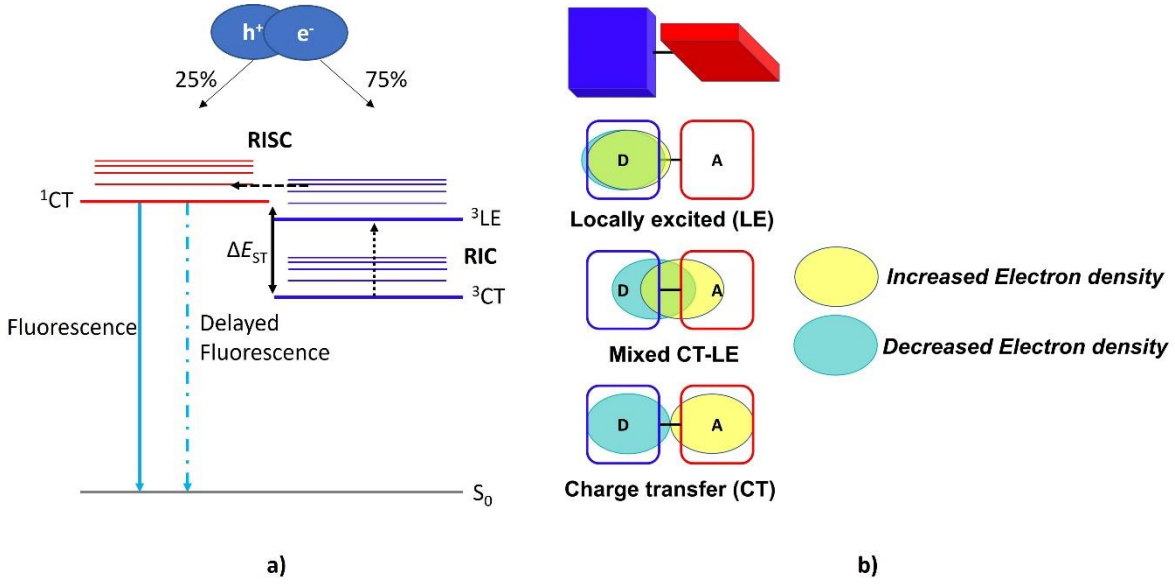


Figure **1**. **a**) Simplified Jablonski diagram showing a TADF mechanism involving spin-vibronic coupling to intermediate triplet states, where $h^+$ is hole, $e^-$ is electron, with $h^+$:$e^-$ the corresponding electron:hole pair created, RISC is reverse intersystem crossing and RIC is reverse internal conversion; **b**) simplified picture of the electronic density distribution of different electronic excited states in a D-A prototypical molecule.

The picture presented in the literature largely supports the existence of pure CT and LE states. Recently, using a combination of molecular dynamics (MD) and excited state calculations using Time-Dependent Density Functional (TD-DFT) within the Tamm-Dancoff approximation (TDA-DFT), some of us demonstrated that the nature of the excited states is often more complex.[20] That work highlighted that excited states are actually mixed between CT and LE, and the degree of mixing is dynamically modulated by the fluctuations of the dihedral angles between the electron donating and accepting units.

The design of TADF emitters has been largely assisted by excited state calculations at the TD-DFT level,[21] either in its full treatment or using TDA-DFT.[22] The use of the latter is now quite well established as a potential solution to addressing the known triplet instability issue inherent in TD-DFT calculations.[23-25] High-throughput screening, particularly in industry, has been adopted as a rapid TADF discovery tool.[26, 27] The screening is often based on the optimization of $\Delta E_{ST}$ in tandem with the oscillator strength. However, this approach largely ignores second-order mixing of excited states and so could miss identifying promising candidates that do not rigorously meet the design criteria of minimizing $\Delta E_{ST}$.

The most common functionals used within the TADF community are hybrid ones that have a low or moderate content of Hartree-Fock like exchange (% HF), such as B3LYP[28] (20% HF) and PBE0[29] (25% HF). The use of these functionals in conjunction with modest-sized basis sets such as 6-31G* typically provide a satisfactory agreement of both the excited state energies and $\Delta E_{ST}$ with the experiment.[23] However, it is important to understand that the calculations do not model either the fluorescence or phosphorescence transitions but rather vertical absorption processes are simulated based on an optimized ground state geometry. Further, nearly all calculations reported in the TADF literature are gas-phase calculations and thus do not take into account the effects of the polarity of the medium, which will more strongly influence the energy of CT states. Long-range functionals such as ωB97XD[30, 31] and LC-ωPBE[32] were developed to improve the description of CT excited states and have initially appeared as alternatives to the previous family of functionals in an effort to more accurately and consistently describe the low-lying CT states present in TADF materials. However, generally, larger $\Delta E_{ST}$ are predicted likely because $S_1$ and $T_1$ possess a larger LE character as compared to PBE0 and B3LYP calculations, resulting in a poorer agreement with the experimental data.[20, 25] A greater degree of accuracy is possible using LC-ωPBE and ωB97XD, where the range-separation parameter, ω, representing the inverse of the distance at which the

exchange term switches from DFT-like to HF like, is optimized for every system (and potentially for every conformation[33]). Adopting this methodology dramatically increases the computational cost for modelling the TADF materials since these functionals become compound and geometry specific. While hybrid functionals, including those containing a low percentage of the Hatree-Fock like exchange, are known to underestimate excited state energies of CT excited states,[25] functionals with higher HF like contributions like the meta-GGA hybrid functionals from the Minnesota family (e.g., 54% for M06-2X) have emerged to address this weakness,[34] without the need to explicitly tune parameters.

Moving beyond DFT calculations, coupled cluster-based methods are considered as some of the most accurate for calculating the properties of ground and excited states of molecules.[35] In particular, the spin-component scaling second-order approximate coupled-cluster (SCS-CC2)[36] calculations used together with the resolution-of-the-identity, have appeared as a cost-effective method to treat molecular systems up to a hundred atoms. SCS-CC2 differs from CC2 by the introduction of different scaling factors for the same-spin and opposite-spin contributions to the correlation energy. SCS-CC2 calculations provide a very high level of accuracy in the predictions of both singlet and triplet energies and $\Delta E_{ST}$, and has been used to great effect when modelling singlet fission[37] and multi-resonant TADF (MR-TADF) materials.[38] SCS-CC2 is not, however, an affordable method for the high-throughput screening of new emitters,[26, 27] for larger systems, or for excited state calculations performed on geometries extracted along a MD trajectory.[20, 39, 40]

Using TD(A)-DFT approaches, several benchmarking studies have been reported with the goal of identifying the most appropriate functionals to use in terms of providing accurate predictions with experiment. Based on a set of six compounds, Moral *et al.*[23] showed that the use of TDA-DFT led to a more accurate prediction of $\Delta E_{ST}$, compared to TD-DFT. Using a larger set of seventeen molecules that possess a wide range of experimental $\Delta E_{ST}$ values, Sun *et al.*[25]

demonstrated that PBE0, M06-2X as well as ω-tuned range-separated functionals such as LC-ωPBE offered excellent agreement between experimental and computed $\Delta E_{ST}$. A recent study by Kunze *et al.* covering twenty-seven TADF emitters across a range of structural classes[41] demonstrated how the use of spin-unrestricted and restricted open-shell Kohn−Sham self-consistent field calculations in combination with a polarizable-continuum can be used to compute with very high accuracy the adiabatic $\Delta E_{ST}$ (MAD of 0.025 eV). Each of these previous studies compared experimental $\Delta E_{ST}$ with the calculated values, and only considered $S_1$ and $T_1$ to evaluate the efficiency of the TADF process. A recent study by Cardeynaels *et al.*[42] probed the modelling of intermediate triplet states of ten D-A emitters by DFT methods and comparing the results to CC2 calculations. This study revealed that M06-2X provided the smallest MAD of 0.13 eV for the absolute energy of $T_2$. Beyond this one report, the comparison between the energies of higher lying triplet states computed at the TD(A)-DFT and a wavefunction-based methodology has not been undertaken.

*An assessment of the efficiency of a TADF emitter must move beyond the simplistic evaluation of $\Delta E_{ST}$, especially given the importance of intermediate excited states to mediate RISC via spin-vibronic coupling.[14, 43, 44] Previous theoretical studies[45] have shown that both $\Delta E_{ST}$ and SOC are in large part governed by the nature of the lowest-lying excited states. The largest $k_{RISC}$ values reported to date have been rationalized using TD-DFT analysis to involve*

*higher-lying triplet states (Figure **2***

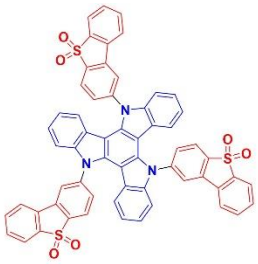

**TAT-3DBTO$_2$**
$k_{RISC}$ = 1.5 × 10$^7$ s$^{-1}$
TDA-PBE0/6-31G(d,p)

*Adv. Sci.*, **2018**, 5, 1700989

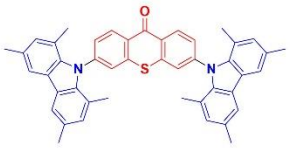

**MCz-TXT**
$k_{RISC}$ = 1.1 × 10$^8$ s$^{-1}$
TDA-LC-ω*BLYP/6-31G(d)

*Sci. Adv.*, **2021**, 7, eabe5769

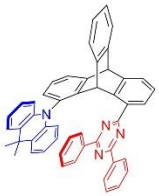

**TpAT-tFFO**
$k_{RISC}$ = 1.2 × 10$^7$ s$^{-1}$
TD-LC-ω*PBE/6-31G(d)

*Nat. Photonics.*, **2020**, 14, 643

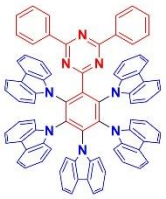

**5Cz-TRZ**
$k_{RISC}$ = 1.5 × 10$^7$ s$^{-1}$
TDA-ω*B97XD/6-31G(d,p)

*Nat. Photonics.*, **2020**, 14, 636

Figure ***2***).[15, 16, 18, 19] However, no universal computational approach exists within the community to either describe these states or their involvement in RISC.

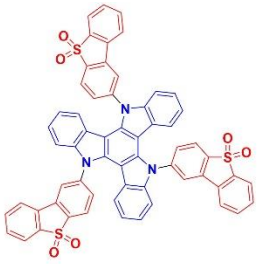

**TAT-3DBTO$_2$**
$k_{RISC}$ = 1.5 × 10$^7$ s$^{-1}$
TDA-PBE0/6-31G(d,p)

*Adv. Sci.*, **2018**, 5, 1700989

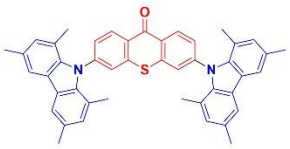

**MCz-TXT**
$k_{RISC}$ = 1.1 × 10$^8$ s$^{-1}$
TDA-LC-ω*BLYP/6-31G(d)

*Sci. Adv.*, **2021**, 7, eabe5769

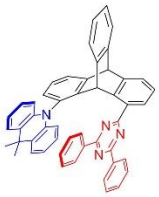

**TpAT-tFFO**
$k_{RISC}$ = 1.2 × 10$^7$ s$^{-1}$
TD-LC-ω*PBE/6-31G(d)

*Nat. Photonics.*, **2020**, 14, 643

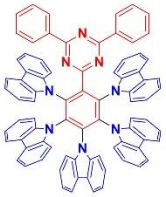

**5Cz-TRZ**
$k_{RISC}$ = 1.5 × 10$^7$ s$^{-1}$
TDA-ω*B97XD/6-31G(d,p)

*Nat. Photonics.*, **2020**, 14, 636

Figure **2**. Structures, experimental $k_{RISC}$ values and DFT method employed to compute the $T_1$ and $S_1$ excited states energies for TADF in these literature-reported emitters.

In the literature, several indices have been developed to quantify the degree of CT in the excited state.[46] The most popular ones rely on the charge transferred ($q_{CT}$) upon excitation, the distance between the hole and electron centroids (Δr), and the overlap between the hole and electron densities based on the attachment-detachment formalism ($\phi_S$).[46] We note here that relying only on a single pair of orbitals to describe the transition to the excited state, and hence these indices, is problematic as the nature of the excited state frequently involves a more complex family of orbital pairs. These indices are better estimated within the Natural Transition Orbital and the attachment-detachment formalisms[47, 48] or directly from an analysis of the difference density[49]

between the ground and excited state, which consider the overall electronic density and not simply the canonical molecular orbitals.

In this study, we have calculated key photophysical properties of fourteen structurally diverse TADF emitters using a range of DFT functionals: B3LYP, PBE0, M06-2X, LC-ωPBE, LC-ω*PBE, LC-ω*HPBE and CAM-B3LYP. We cross-compared the predictions from these calculations to those using SCS-CC2 in order to determine the optimal DFT methodology for the modelling of donor-acceptor TADF emitters.

### 2.1 Methodology

All the quoted excited states energies were obtained from vertical excitations based on the optimized ground state geometry. All calculations were carried out in the gas-phase. Notably, there is a diversity of conditions, media and methods used to experimentally determine $\Delta E_{ST}$, which introduces a certain degree of variability in the values reported. Compounds were optimized using the following DFT functionals: PBE0;[29] CAM-B3LYP;[50] B3LYP;[28] LC-ωPBE;[32] ω-tuned LC-ωPBE[25] (LC-ω*PBE); ω-tuned LC-ωHPBE[51] (LC-ω*HPBE); and M06-2X.[34] Each of these functionals was used in conjunction with the D3(BJ)[52] dispersion correction scheme and the 6-31G(d,p)[53] basis set. This basis set is widely employed in TD-DFT studies and thus also in the TADF literature. Following the initial ground state optimization, vertical excitations were calculated using both TD-DFT and TDA-DFT approaches. Additionally, for each compound, both the ground state geometry optimization and the vertical excitations were calculated at the SCS-CC2[54-56] level with the cc-pVDZ[57] basis set. The choice of this Dunning basis set is appropriate for wavefunction-based approaches and keeps the computational cost relatively low.[58] Although cc-pVDZ is relatively small, previous work has highlighted that this basis performs similarly to larger basis sets such as def2-TZVP.[38] The energies and nature of $S_1$, $T_1$ as well as $T_2$ were calculated using both TD(A)-DFT and SCS-CC2. TD(A)-DFT

calculations were performed using Gaussian 09,[59] or Gaussian 16[60] when the LC-ω*HPBE was considered, while SCS-CC2 calculations were performed using Turbomole 7.4 package.[61]

In both LC-ω*PBE and LC-ω*HPBE methods, the range separation parameter, ω, was optimized in order to minimize the error $J^2$, defined as:

$$J^2 = \sum_{i=0}^{1}[\varepsilon_H(N+i) + IP(N+i)]^2 \quad (2)$$

where $\varepsilon_H(N+i)$ and $IP(N+i)$ are the HOMO energy and the ionization potential of a N-electron system (i.e., the ground state) and N+1-electron system (i.e., the radical anion). The vertical electron affinity is assumed to be equivalent to the ionization potential of the N+1-electron system. Such an approach offers a quite accurate estimate of the $S_1$ excitation energy and the $\Delta E_{ST}$ at the expense of the optimization of the ω parameter.

As the TADF process depends on the energy difference between excited states and not on their absolute value, we placed a particular emphasis on the comparison of the differences in energy, between $S_1$ and $T_1$ ($\Delta E_{ST}$), between $S_1$ and $T_2$ ($\Delta E_{S1T2}$) and between $T_1$ and $T_2$ ($\Delta E_{T1T2}$). We note that in some cases, more than one intermediate triplet state is present between $T_1$ and $S_1$; however, these are not explicitly accounted for in this study. We note that the greater density of intermediate triplet excited states should lead to an enhancement of the RISC rate.[62, 63]

The nature of the excited states at the TD(A)-DFT level was determined by analysis of the $\phi_S$ index, which refers to the overlap between the attachment ($\rho_A$) and detachment ($\rho_D$) densities that are associated with the hole and electron densities, respectively. $\phi_S$ varies between 0, where there is no overlap between the hole and electron densities and indicates that the excitation is CT, and 1, where there is complete overlap of the hole and electron densities and indicates that the excitation is LE (Figure **3**).[46] Values between the two represent excitations bearing a mixed CT-LE character. The $\phi_S$ values were obtained through a post-analysis of Gaussian outputs

with the NANCY-EX 2.0 software.[64, 65] In the analysis of the SCS-CC2 wavefunctions, we rely on the difference density, $\Delta\rho$, computed as the difference between the excited state, $\rho_{EX}$, and the ground state, $\rho_{GS}$, densities, to characterize the nature of the excited states.

At the TD(A)-DFT level, the difference density $\Delta\rho$ is readily obtained by computing the difference $\Delta\rho$ between the attachment $\rho_A$ and the detachment $\rho_D$ densities.[47]

Using $\Delta\rho$, several metrics to study the CT character of excited states have been investigated using the Multiwfn 3.6 software.[66] Following the work by Le Bahers *et al.*, two functions, $\rho_+$ and $\rho_-$, are defined to account for the increase and decrease in density upon electronic excitation, which reflect $\rho_{EX}$ and $\rho_{GS}$, respectively.[67] The calculation of these metrics based on $\Delta\rho$, computed either at the TD(A)-DFT and SCS-CC2 levels, allow for a straightforward comparison between the two approaches. To facilitate the comparison between TD(A)-DFT and SCS-CC2, we compared the single electron difference density obtained at the SCS-CC2 level, omitting the second-order contribution.

The first metric, $D_{CT}$, is defined as the distance between the barycentres, $R_+$ and $R_-$, of the two density components, $\rho_+(r)$ and $\rho_-(r)$, characterizing an increase or a decrease of the electronic density at point r of space, respectively.[49, 68] The larger $D_{CT}$ the greater the CT character of the excited state; however, problems can arise in centrally symmetric systems, where the calculation of the barycentre associated with a given excitation suggests a state of LE character, leading to a zero value for $D_{CT}$ while the other indices ($\phi_S$, $q_{CT}$, *vide infra.*) imply a state of a CT character.[46, 49] Thus, it is advisable to employ another descriptor. The charge transferred (in number of electrons), $q_{CT}$, relates to the integration of $\rho_+$ (or $\rho_-$), over all space. The larger the number, the greater the extent of electronic rearrangement. A value of 0 signifies a state that is pure LE while a value of 1 is associated with a purely CT state.[67]

The final metrics employed is the overlap ($S_{+-}$) between centroids of charges associated with positive ($C_+$) and negative ($C_-$) density, with $C_+$ and $C_-$ defined as:

$$C_+(r) = A_+ e\left(-\frac{(x-x_+)^2}{2\sigma^2{}_{+x}} - \frac{(y-y_+)^2}{2\sigma^2{}_{+y}} - \frac{(z-z_+)^2}{2\sigma^2{}_{+z}}\right) (3)$$

$$C_-(r) = A_- e\left(-\frac{(x-x_-)^2}{2\sigma^2{}_{-x}} - \frac{(y-y_-)^2}{2\sigma^2{}_{-y}} - \frac{(z-z_-)^2}{2\sigma^2{}_{-z}}\right) (4)$$

Where $A_+$ and $A_-$ are the normalization factors chosen to impose the integrated charge on the centroid to be equal to the corresponding density change integrated in the whole space. The overlap between these two points $C_+$ and $C_-$ provides $S_{+-}$. A value equal to 1 indicates $C_+$ and $C_-$ completely overlap, while a value of 0 indicates they are completely disconnected, corresponding to LE and CT electronic transitions respectively (Figure ***3***).

In this study, we will cross-compare the three metrics calculated from Δρ using SCS-CC2 and the DFT method using each of the aforementioned functionals.

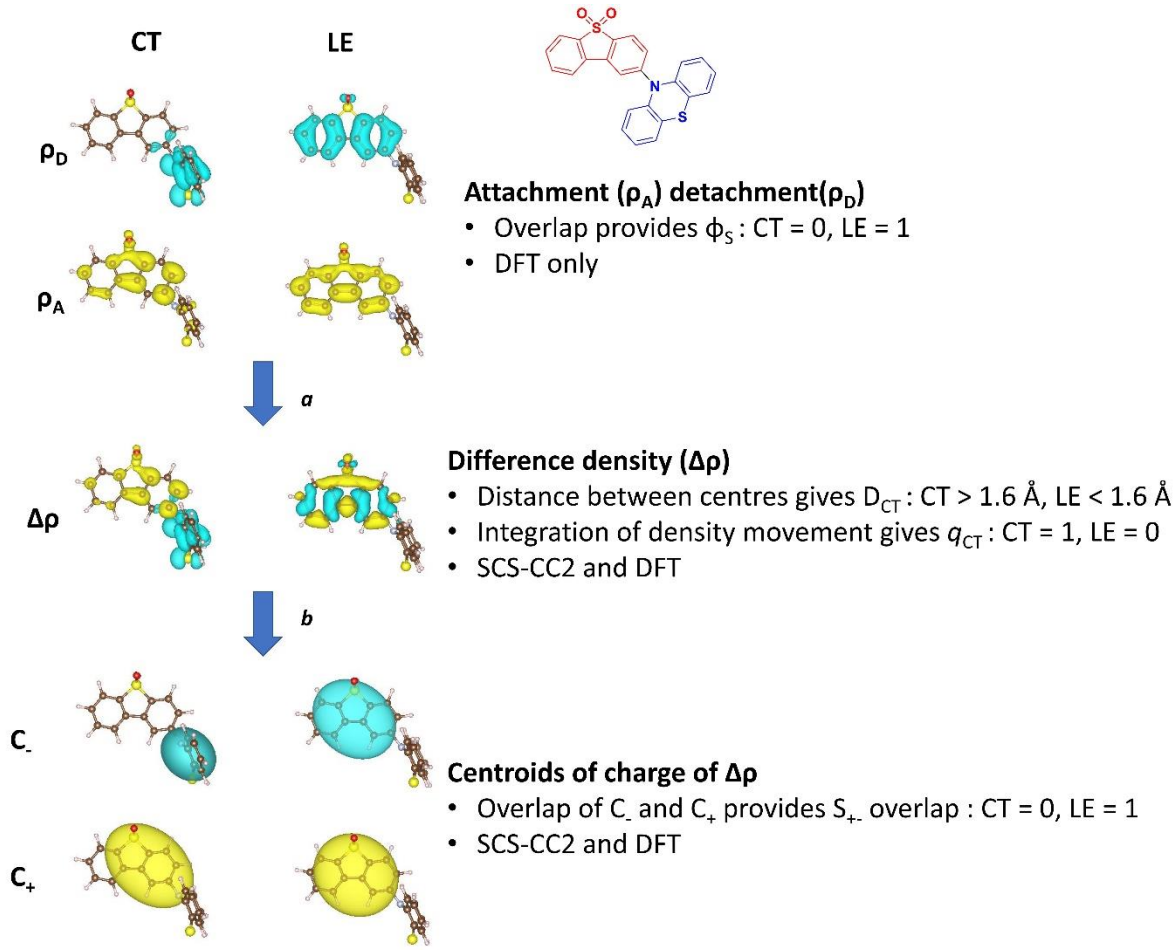


Figure **3**. Pictures of the electronic density associated with a given excited state and the corresponding metrics to quantify the degree of CT for a representative donor-acceptor TADF

compound, **PTZ-DBTO2** using each of the different methods (see text). Each density was calculated using TDA-CAM-B3LYP/6-31G(d,p).

To assess the predictive accuracy of each DFT functional against SCS-CC2, we report on the mean average deviation (MAD), root mean square deviation (RMSD) and standard deviation (σ) for $S_1$, $T_1$, $T_2$, $\Delta E_{ST}$, $\Delta E_{S1T2}$, $\Delta E_{T1T2}$, $q_{CT}$, $D_{CT}$ and $S_{+-}$ for each of the fourteen compounds. These are computed following the definitions in equations 6-8:

$$\text{MAD} = \frac{1}{n}\sum_{i=1}^{n}|x_i| \qquad (6)$$

$$\text{RMSD} = \sqrt{\frac{1}{n}\sum_{i=1}^{n}|x_i|^2} \qquad (7)$$

$$\sigma = \sqrt{(\frac{1}{n}\sum_{i=1}^{n}|x_i|^2) - (\frac{1}{n}\sum_{i=1}^{n}|x_i|)^2} \qquad (8)$$

where $x_i = y_i^{DFT} - y_i^{SCS-CC2}$, $y_i^{DFT}$being $S_1$, $T_1$, $T_2$, $\Delta E_{ST}$, $\Delta E_{S1T2}$, $\Delta E_{T1T2}$ $q_{CT}$, $D_{CT}$ or $S_{+-}$ calculated at the TD(A)-DFT level and $y_i^{SCS-CC2}$ the corresponding SCS-CC2 energy, energy difference or nature, with the *i* index running over the series of n=14 studied molecules.[69]

### 2.2 Emitters in the study

The fourteen structurally diverse emitters are representative TADF compounds that show a range of photophysical behaviour (e.g., $\Delta E_{ST}$ ranging from 0.01 eV and 0.22 eV). The chemical structures are shown in Figure **4**, and the photophysical properties and OLED performance are collated in Table **S1**.

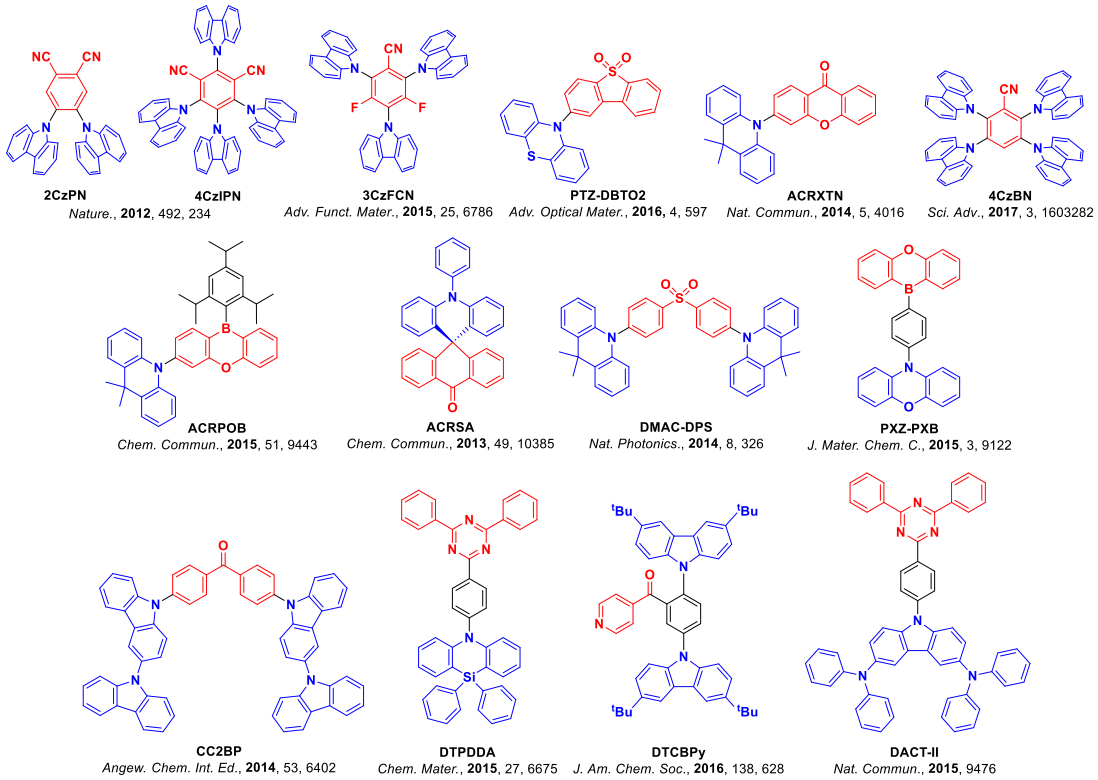


Figure **4**. Chemical structures of the TADF emitters in this study. Blue components represent donor units and red components represent acceptor units.

## 3. Discussion and Results

### 3.1. Excited-state energies

We started by investigating the energies of $S_1$, $T_1$ and $T_2$ (Figure **S1** – **S4**, Tables **S2** – **S15**). There is an evident and consistent underestimation of the excited states energies for B3LYP and PBE0 with both TD-DFT and TDA-DFT compared to SCS-CC2. This is due to the over stabilisation of CT states, which has been widely reported,[46] and mainly arises from self-interaction errors due to a low content of HF like exchange which is evident in the large MAD values (Table **1**) for $S_1$, $T_1$ and $T_2$. For both B3LYP and PBE0 a slightly improved MAD is achieved for both triplet states using TDA-DFT compared with TD-DFT, which is due to an improved triplet character description. The $S_1$ state is predicted with a similar level of accuracy

using either TD-DFT or TDA-DFT. Indeed, TD-DFT and TDA-DFT are formally equivalent when the excited states bear a strong CT character as usually observed for the $S_1$ state of D-A TADF materials. A smaller standard deviation is thus reported for both $T_1$ and $T_2$ than for $S_1$ because the exchange interaction tends to increase the LE character (decrease the CT character) of these latter states in comparison to $S_1$. This is further stressing the systematic excited states overstabilization of excited states energies with strong CT obtained with low HF exchange functionals. The use of M06-2X results in vastly improved excited state energy prediction for $T_1$, $T_2$ and $S_1$, with a reduced MAD for each compound compared to SCS-CC2 (Table **1**). This is due to the increased HF like contribution in this functional, which improves the description of CT excited states. Excellent agreement for both $T_1$ and $T_2$ is obtained for TDA-DFT calculations using LC-ωPBE without tuning ω, while TD-DFT calculations using the same functional largely underestimate the $T_1$ energies. This is likely due to the more accurate description of states with significant LE character using this functional while states with significant CT character are not well described. The ω-tuned LC-ω*PBE (LC-ω*HPBE) functionals partially address the issue observed with LC-ωPBE, leading to a decrease in $T_1$ and $T_2$ MADs, especially at the TDA-DFT level (see Table ***1***). The MAD for $S_1$ is very similar for both LC-ω*PBE and LC-ω*HPBE using either TD-DFT or TDA-DFT. The use of TDA-CAM-B3LYP results in a closer agreement with SCS-CC2 than with TD-CAM-B3LYP, which essentially comes from an improved description of LE-dominated triplet states. The $S_1$ energy is also well predicted with CAM-B3LYP as this functional has been designed to more accurately describe CT states. Based on this analysis, it is clear that TDA-DFT calculations are more accurate than TD-DFT calculations, in agreement with previous findings.[23, 25] Both M06-2X and CAM-B3LYP calculations produce the smallest MAD and smallest standard deviation to the SCS-CC2 results. The summary of MAD, RMSD and σ are found in Table **1**, Figure **5** and Figure **S5**.

Table **1**. MAD, RMSD and σ on the energies of the investigated excited states in comparison to SCS-CC2.

| | $S_1$ / eV | | | $T_1$ / eV | | | $T_2$ / eV | | |
|---|---|---|---|---|---|---|---|---|---|
| | **MAD** | **RMSD** | **σ** | **MAD** | **RMSD** | **σ** | **MAD** | **RMSD** | **σ** |
| **TD - CAM-B3LYP** | 0.10 | 0.12 | 0.06 | 0.46 | 0.46 | 0.07 | 0.47 | 0.50 | 0.15 |
| **TDA - CAM-B3LYP** | 0.10 | 0.13 | 0.08 | 0.12 | 0.14 | 0.08 | 0.15 | 0.17 | 0.08 |
| **TD - LC-ωPBE** | 0.56 | 0.61 | 0.25 | 0.76 | 0.77 | 0.09 | 0.82 | 0.83 | 0.16 |
| **TDA - LC-ωPBE** | 0.61 | 0.67 | 0.26 | 0.09 | 0.11 | 0.06 | 0.13 | 0.17 | 0.10 |
| **TD - LC-ω*PBE** | 0.45 | 0.47 | 0.14 | 0.52 | 0.53 | 0.10 | 0.56 | 0.57 | 0.10 |
| **TDA - LC-ω*PBE** | 0.43 | 0.46 | 0.14 | 0.46 | 0.48 | 0.14 | 0.48 | 0.49 | 0.11 |
| **TD - LC-ω*HPBE** | 0.45 | 0.47 | 0.13 | 0.52 | 0.53 | 0.10 | 0.56 | 0.57 | 0.10 |
| **TDA - LC-ω*HPBE** | 0.44 | 0.46 | 0.14 | 0.46 | 0.48 | 0.14 | 0.48 | 0.49 | 0.11 |
| **TD - B3LYP** | 1.03 | 1.06 | 0.24 | 0.89 | 0.91 | 0.18 | 0.80 | 0.81 | 0.14 |
| **TDA - B3LYP** | 1.03 | 1.06 | 0.23 | 0.89 | 0.90 | 0.17 | 0.76 | 0.78 | 0.17 |
| **TD - PBE0** | 0.85 | 0.88 | 0.21 | 0.77 | 0.78 | 0.12 | 0.74 | 0.74 | 0.11 |
| **TDA - PBE0** | 0.84 | 0.87 | 0.21 | 0.72 | 0.74 | 0.15 | 0.63 | 0.65 | 0.13 |
| **TD - M06-2X** | 0.15 | 0.18 | 0.10 | 0.15 | 0.19 | 0.12 | 0.18 | 0.20 | 0.08 |
| **TDA - M06-2X** | 0.12 | 0.14 | 0.07 | 0.12 | 0.16 | 0.11 | 0.12 | 0.14 | 0.08 |

### 3.2. Relative Energy Differences

We now turn to the prediction of the energy differences between excited states, values that are relevant when ascertaining $k_{RISC}$. Despite the large overstablization of the excited state energies computed with PBE0 and B3LYP at both TD-DFT and TDA-DFT, the MADs for $\Delta E_{ST}$ are small, see Table **2**. This is due to the large but similar errors computed for $T_1$ and $S_1$. However, the MADs for $\Delta E_{S1T2}$ and $\Delta E_{T1T2}$ and their associated standard deviations are much larger than for the other functionals (Table **2**). Specifically, in five examples (**PXZ-PXB**, **PTZ-DB2OT**, **DTPDDA**, **DTCBPy** and **DACT-II**) $T_2$ is predicted to be higher in energy than $S_1$ using DFT

methods while this is not observed with SCS-CC2. Each of these five compounds displays $S_1$ and $T_1$ states that have large CT character, both of which are stabilized compared to other low-lying excited states (*vide infra*). $\Delta E_{ST}$, $\Delta E_{S1T2}$ and $\Delta E_{T2T1}$ computed with M06-2X (using either TDA-DFT or TD-DFT) are all very close to those computed with SCS-CC2. The smaller MAD at the TDA-DFT compared to TD-DFT is again ascribed to the former handling better the known triplet instability issue.

$\Delta E_{ST}$ and $\Delta E_{S1T2}$ show large MAD values when the functional LC-ωPBE is used at both TDA-DFT and TD-DFT levels, in line with the larger MAD for $S_1$ energy calculations in comparison to both the MADs of $T_1$ and $T_2$ excited states energies. For both TDA-DFT and TD-DFT calculations, by tuning ω in the LC-ω*PBE and LC-ω*HPBE functionals, all relative energy differences are now in good agreement with the corresponding ones computed at the SCS-CC2 level, owing to a much better handling of CT states that is reflected in the largely stabilized $S_1$. TDA-CAM-B3LYP calculations for $\Delta E_{ST}$, $\Delta E_{S1T2}$ and $\Delta E_{T2T1}$ are in good agreement with those using SCS-CC2. In contrast, the MAD values for $\Delta E_{ST}$ and $\Delta E_{S1T2}$ are much larger using TD-CAM-B3LYP. The similar MAD value for $\Delta E_{T1T2}$ at both TD-DFT and TDA-DFT levels suggest that TDA acts similarly on both $T_1$ and $T_2$. Overall, this study reveals the importance for the use of TDA-DFT when employing CAM-B3LYP in order to predict accurately the relative energies of the low-lying excited states.

Based on the calculations of both the absolute and relative energies of the excited states, we can conclude that functionals containing a lower HF-like exchange content such as PBE0 and B3LYP are not appropriate. M06-2X provides a much better description of the excited state energies. The use of CAM-B3LYP within the TDA-DFT approximation is also an appropriate methodology. LC-ωPBE is also not recommended to be used as it offers a poorly described excited state picture, mainly due to the problematic prediction of the $S_1$ energy. Tuning of ω improves significantly the prediction of $S_1$, and both LC-ω*PBE and LC-ω*HPBE perform

essentially identically. However, our current investigation tends to show that relying on range-separated functionals for which ω is tuned might not be needed to obtain a reliable excited state picture of D-A TADF emitters. Indeed, alternatives such as M06-2X and CAM-B3LYP show comparable accuracies to LC-ω*PBE and LC-ω*HPBE and are thus recommended when evaluating the relative energies between excited states. A full summary of MAD, RMSD and σ is found in Table **2**, Figure **5** and Figure **S5**.

Table **2**. MAD RMSD and σ of the energy differences between the considered excited states in comparison to SCS-CC2.

| | $\Delta E_{ST}$ / eV | | | $\Delta E_{S1T2}$ / eV | | | $\Delta E_{T2T1}$ / eV | | |
|---|---|---|---|---|---|---|---|---|---|
| | **MAD** | **RMSD** | **σ** | **MAD** | **RMSD** | **σ** | **MAD** | **RMSD** | **σ** |
| **TD - CAM-B3LYP** | 0.49 | 0.50 | 0.12 | 0.50 | 0.52 | 0.15 | 0.10 | 0.14 | 0.09 |
| **TDA - CAM-B3LYP** | 0.17 | 0.19 | 0.10 | 0.19 | 0.21 | 0.09 | 0.05 | 0.06 | 0.04 |
| **TD - LC-ωPBE** | 1.32 | 1.34 | 0.26 | 1.37 | 1.39 | 0.23 | 0.13 | 0.16 | 0.09 |
| **TDA - LC-ωPBE** | 0.65 | 0.68 | 0.19 | 0.66 | 0.70 | 0.23 | 0.10 | 0.12 | 0.07 |
| **TD - LC-ω*PBE** | 0.12 | 0.15 | 0.09 | 0.13 | 0.15 | 0.07 | 0.07 | 0.09 | 0.06 |
| **TDA - LC-ω*PBE** | 0.12 | 0.15 | 0.08 | 0.11 | 0.12 | 0.05 | 0.10 | 0.12 | 0.06 |
| **TD - LC-ω*HPBE** | 0.12 | 0.14 | 0.09 | 0.13 | 0.15 | 0.07 | 0.07 | 0.10 | 0.06 |
| **TDA - LC-ω*HPBE** | 0.12 | 0.15 | 0.08 | 0.11 | 0.12 | 0.05 | 0.10 | 0.12 | 0.06 |
| **TD - B3LYP** | 0.15 | 0.19 | 0.12 | 0.26 | 0.34 | 0.21 | 0.19 | 0.24 | 0.15 |
| **TDA - B3LYP** | 0.16 | 0.20 | 0.13 | 0.29 | 0.39 | 0.26 | 0.23 | 0.29 | 0.18 |
| **TD - PBE0** | 0.13 | 0.17 | 0.11 | 0.20 | 0.24 | 0.13 | 0.14 | 0.18 | 0.12 |
| **TDA - PBE0** | 0.14 | 0.19 | 0.12 | 0.27 | 0.34 | 0.21 | 0.21 | 0.24 | 0.13 |
| **TD - M06-2X** | 0.13 | 0.16 | 0.10 | 0.14 | 0.20 | 0.14 | 0.09 | 0.12 | 0.07 |
| **TDA - M06-2X** | 0.11 | 0.15 | 0.10 | 0.10 | 0.12 | 0.07 | 0.09 | 0.12 | 0.07 |

### 3.3. Oscillator strength

The oscillator strength was calculated for each singlet state, (Figure **S6** and Table **S16**). There were consistent predictions across the series of functionals (MAD < 0.05); however, σ ranged

more widely from 0.04 to 0.12. A slight improvement was found when using TD-DFT compared to TDA-DFT. Despite their poorly described excited states, B3LYP, PBE0 and LC-ωPBE provide the smallest MAD and σ.

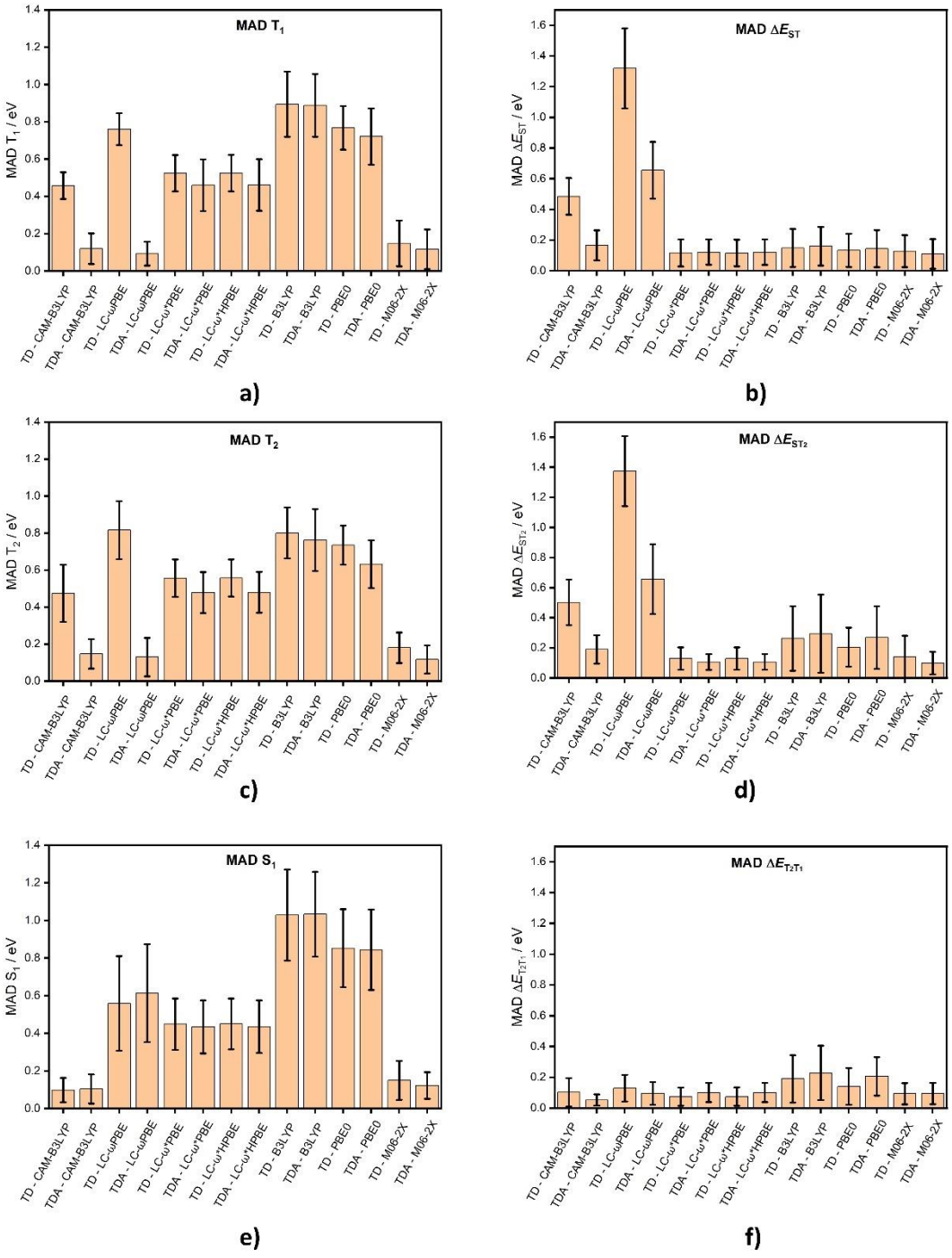


Figure **5**. MAD and σ for each functional in comparison to SCS-CC2, where **a)** is $T_1$, **b)** $\Delta E_{ST}$, **c)** $T_2$, **d)** $\Delta E_{ST2}$, **e)** $S_1$, and **f)** $\Delta E_{T2T1}$.

## 4. Nature of Excited states

The nature of each of the excited states was determined, and a full summary of the $\phi_S$, $q_{CT}$, $D_{CT}$ and $S_{+-}$ metrics is found in the supporting information ($\phi_S$ values for each emitter, Tables **S17** – **S30** and Figures **S7** – **S10**; $q_{CT}$, $D_{CT}$ and $S_{+-}$ values, Tables **S31** – **S44** and Figures **S13** – S**24**). We computed the MAD, the RMSD and the standard deviation for the difference in the metrics between TD(A)-DFT and SCS-CC2 for each excited state ($S_1$, $T_1$ and $T_2$, Tables **S45** – **S47**).

### 4.1 $\phi_S$ of DFT functionals

For most emitters, the $S_1$ state is predicted to be more CT-like compared to $T_1$, (lower $\phi_S$ values) as the exchange interaction increases the spatial confinement of triplet states and thus their LE character. Across all emitters in this study a modest increase in the CT character of the $S_1$ state is observed when TDA-DFT is used instead of TD-DFT. This is due to the fact that TD-DFT reduces to TDA-DFT when excited states with a large CT character are computed.[23] Interestingly, when tracking the nature of the two lowest triplet excited states, we sometimes observe a state inversion depending on the use of either TD-DFT or TDA-DFT. This is particularly evident for **DTPDDA** (Figure **S9d**), where LC-ω*PBE, LC-ω*HPBE and M06-2X at TD-DFT predict a $T_1$ state with a LE character ($\phi_S > 0.8$), while $T_2$ remains mainly CT ($\phi_S < 0.4$). However, when TDA-DFT is employed, the $T_1$ is now a CT state ($\phi_S < 0.4$) with a nature that is very similar to those of $T_2$ calculated using TD-DFT, while $T_2$ becomes LE ($\phi_S > 0.8$). These two states are very close in energy to each other (between 0.09 eV and 0.13 eV), with the LE state being pushed above the CT state in TDA-DFT because of its better handling of the triplet instability issue.

The PBE0 and B3LYP functionals display very similar $\phi_S$ values and tend to predict $T_1$ and $T_2$ states to have an increased CT character in comparison to the other functionals. LC-ωPBE

appears to be the outlier functional, often resulting in a much larger $\phi_S$ value. As an example, **PXZ-PXB** has a predicted $\phi_S$ value for $S_1$ of > 0.7 while all other DFT functionals predict $\phi_S$ < 0.3 (Figure **S10b**). This is evidence of one of the potential issues encountered with long-range corrected functionals, which tend to destabilize CT states. CAM-B3LYP, LC-ω*PBE, LC-ω*HPBE and M06-2X consistently report very similar $\phi_S$ values for the $S_1$ state across the family of emitters in this study, irrespective of whether TD-DFT or TDA-DFT is used. For the triplets, we see a larger spread in $T_1$ and $T_2$ $\phi_S$ values predicted by the CAM-B3LYP, LC-ω*PBE, LC-ω*HPBE and M06-2X functionals compared to $S_1$.

### 4.2 Comparison of the nature of the excited states as predicted using TD(A)-DFT and SCS-CC2

In this section, we embark on a comparison of the nature of the excited states between the different functionals and our reference method SCS-CC2. The nature of the excited state is predicted on the basis of a post-analysis of the difference density. To do so we convert from an attachment-detachment formalism to a difference density picture for all excited states obtained at the TD(A)-DFT level. We compare this picture to the difference density computed at the SCS-CC2 level.

#### 4.2.1 Singlet state

The nature of the $S_1$ state calculated using DFT and SCS-CC2 methods was compared by computing the $q_{CT}$, $D_{CT}$ and $S_{+-}$ of $S_1$ descriptors. While TD(A)-DFT and SCS-CC2 predict a $S_1$ state with a dominant CT character for essentially all the emitters, one clear outlier exists in terms of **DACT-II**. For this emitter TD(A)-DFT predicts an excited state with largely CT

character, while SCS-CC2 predicts that this state contains mainly LE character. Interestingly, the $S_2$ excited state predicted by TD(A)-DFT is LE-like while SCS-CC2 calculations suggest it is a CT state, which reflects an inversion of $S_1$ and $S_2$ (see difference density plots in Figure **6** and Table **S25**); the energy difference between $S_1$ and $S_2$ is small at 0.06 eV using SCS-CC2 while at the TD(A)-DFT, this energy difference is larger, ranging at 0.08 eV to 0.31 eV. Because of this states inversion, the data corresponding to **DACT-II** were removed from the averages on the overall collective data.

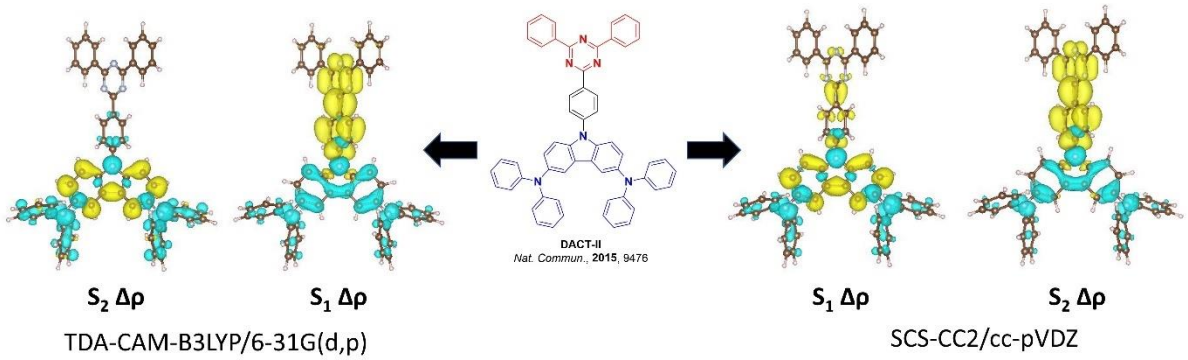


Figure **6**. Change in Δρ singlet picture for **DACT-II** between (left) TDA-CAM-B3LYP/6-31G(d,p) and SCS-CC2/cc-pVDZ (right) calculations.

The evaluation of the CT descriptors for the set of compounds confirms the close agreement between CAM-B3LYP and SCS-CC2 for the nature of the $S_1$ state. The other range-separated functional, LC-ωPBE does not perform as well ,with large MAD and σ values for $q_{CT}$, $D_{CT}$ and $S_{+-}$ (Tables **3-5**), which are associated with predicted state inversion in **ACRXTN**, **DTCBPy**, **PTZ-DBTO2** and **PXZ-PXB**. When either LC-ω*PBE and LC-ω*HPBE are used, there is close agreement for the description of $S_1$ and its associated energy with those computed by SCS-CC2. Neither PBE0 nor B3LYP at TD-DFT and TDA-DFT accurately predict the nature of the excited states (Tables **3 – 5**). Their overestimation of the CT character explains the heavily stabilized $S_1$ energy values reported for the absolute energies. Finally, the M06-2X

functional provides a similar and equally accurate picture of the nature of $S_1$ with that of CAM-B3LYP. Based on this analysis, we would encourage the community to use either CAM-B3LYP, M06-2X, LC-ω*PBE or LC-ω*HPBE to obtain accurate predictions of the nature and energy of the $S_1$ state.

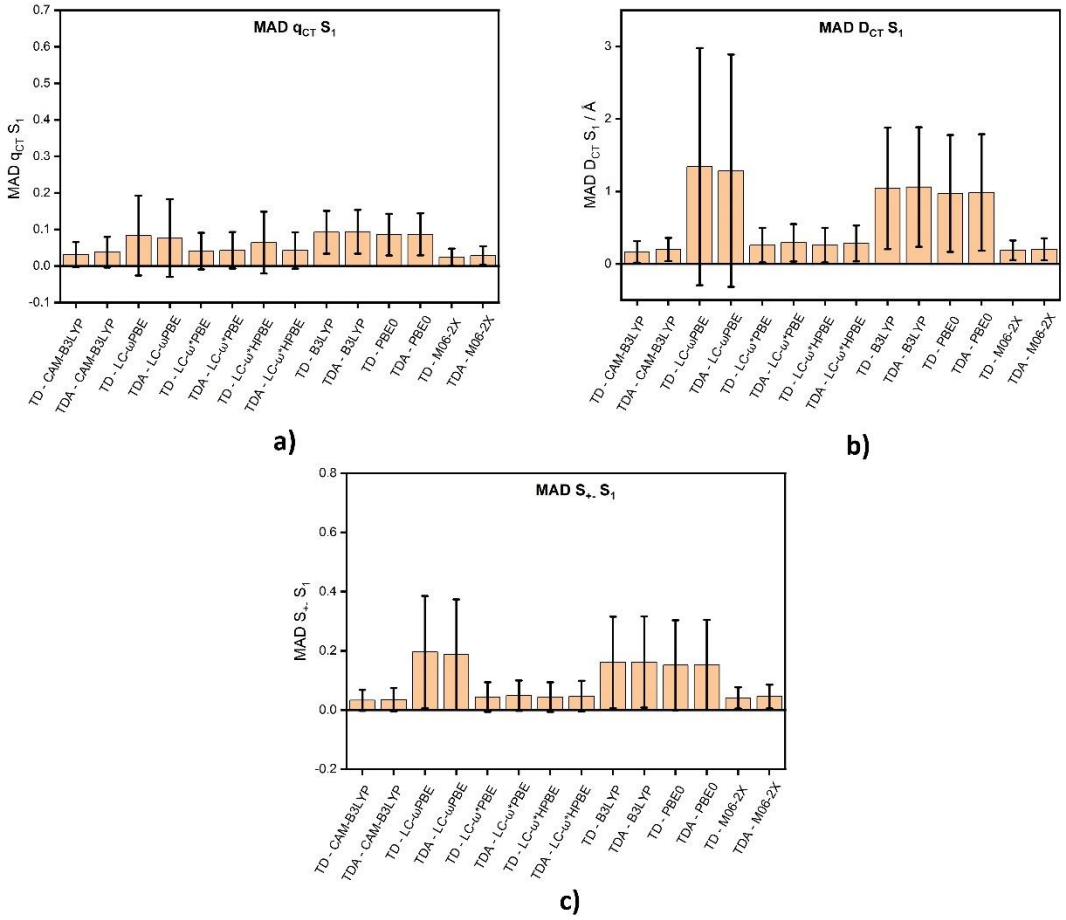


Figure **7**. MAD data for the $S_1$ state nature between TD(A)-DFT and SCS-CC2 calculations, where **a**) is $q_{CT}$, **b**) is $D_{CT}$ and **c**) is $S_{+-}$

### 4.2.2 Triplet states

We next discuss the data associated with the prediction of the triplet state character. The nature of $T_1$ as computed at TDA-CAM-B3LYP is closer to the one predicted with SCS-CC2 than at the TD-CAM-B3LYP level (see CT metrics reported in Tables **S45** to **S47**). However, the

opposite is observed for $T_2$, wherein the MAD values of the CT descriptors increase when moving from TDA-DFT to TD-DFT. Overall, it should be noted that the $T_1$ and $T_2$ MAD values are significantly larger than the respective $S_1$ observations.

LC-ωPBE does a poor job in predicting the nature of both $T_1$ and $T_2$; still, the use of TDA improved the MAD for each excited state descriptor compared to TD-DFT. Unfortunately, neither the use of LC-ω*PBE nor LC-ω*HPBE produced a more accurate descriptor of the triplet state character (MAD values similar to those of LC-ωPBE) despite there being a significant improvement in the quality of the energy prediction.

As for $S_1$, both B3LYP and PBE0 produce erroneous $T_1$ and $T_2$ assignments as the CT character of these states is overestimated. Inclusion of greater HF like contribution within M06-2X improves the triplet description, though the discrepancy compared to SCS-CC2 is much larger than that observed for the description of the $S_1$ state.

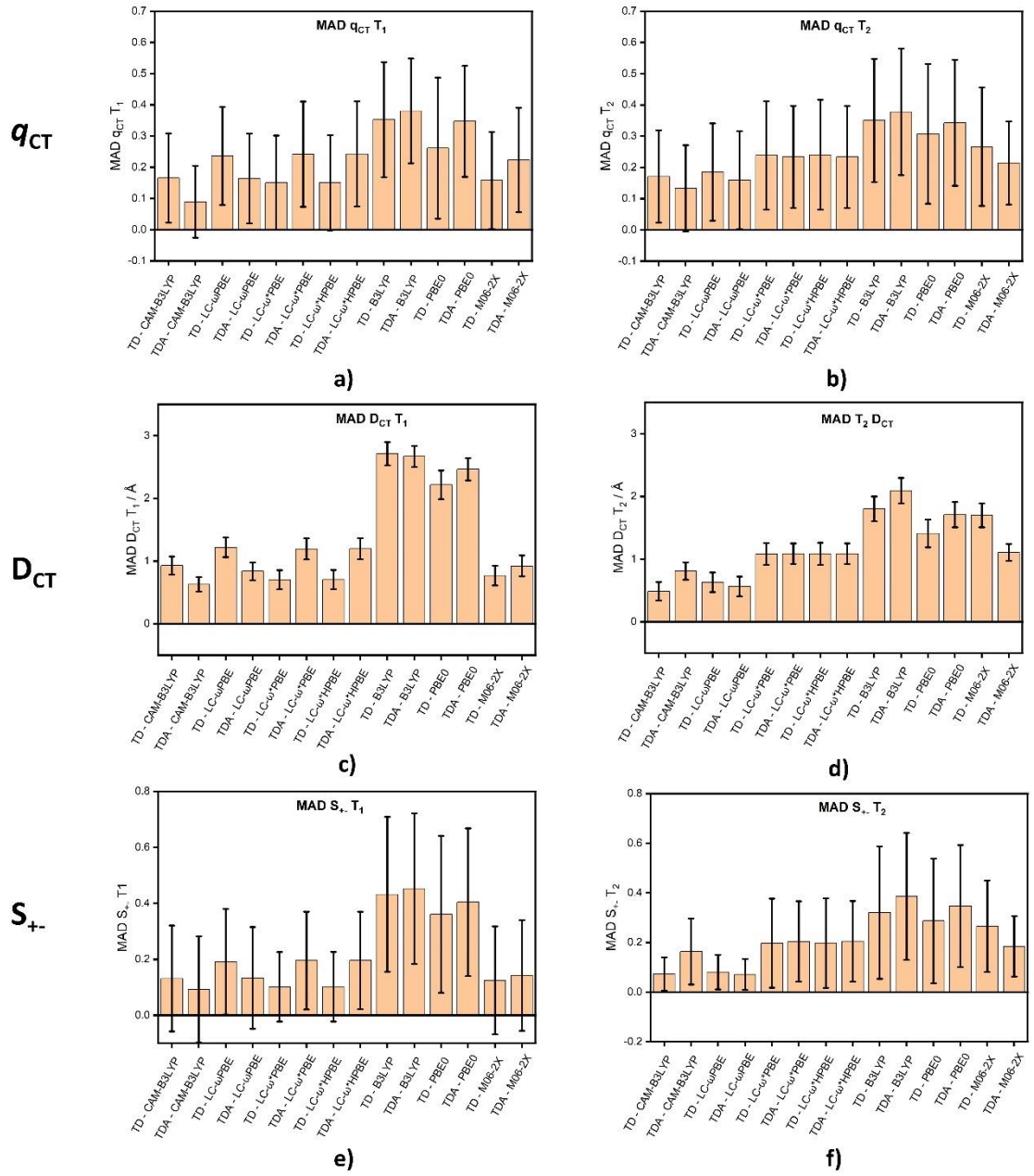


Figure **8**. MAD data for the $T_1$ (left) and the $T_2$ (right) states nature between TD(A)-DFT and SCS-CC2 calculations, where **a**) and **b**) are $q_{CT}$, **c**) and **d**) are $D_{CT}$ and **e**) and **f**) are $S_{+-}$

## 5 Conclusions

We have compared the results of DFT calculations across a series of commonly used functional to predictions made using SCS-CC2 of (i) vertical excitation energies, (ii) vertical excitation energy differences and (iii) nature of excited states for a series of fourteen TADF emitters. The

objective of our study was to determine the best choice of functional for modelling the optoelectronic properties of donor-acceptor TADF compounds. We observed that TDA-DFT calculations provided a more accurate prediction of the vertical excitation energies compared to TD-DFT, as has been previously documented.[23, 25] Both TDA-M06-2X and TDA-CAM-B3LYP calculations provide very good agreement for $S_1$, $T_1$ and $T_2$; TDA-LC-ωPBE calculations produce reasonably accurate $T_1$ and $T_2$ energies, but consistently overestimate the $S_1$ energy. B3LYP, PBE0 and the ω-tuned functionals consistently underestimate triplet and singlet state energies, resulting in large deviations from the SCS-CC2 calculations. When considering excited state energy gaps, TDA-LC-ωPBE and TD-DFT-LC-ωPBE calculations produce large deviations in both $\Delta E_{ST}$ and $\Delta E_{ST2}$, the result of the much larger MAD for $S_1$ than for $T_1$ and $T_2$. $\Delta E_{T2T1}$ is much better reproduced for most functionals in comparison with $\Delta E_{ST}$ and $\Delta E_{ST2}$. However, PBE0 and B3LYP show comparable MADs but larger standard deviations when evaluating $\Delta E_{T2T1}$ questioning their reliability in predicting this parameter. Of the functionals evaluated, TDA-M06-2X and TDA-CAM-B3LYP offer the most accurate predictions, evidenced by their low MAD for $\Delta E_{ST}$ $\Delta E_{ST2}$ and $\Delta E_{T2T1}$; the MAD values increased for the analogous TD-DFT calculations as here the triplet states are overstabilized.

Finally, we investigated the nature of the excited states, computing the $q_{CT}$, $D_{CT}$ and $S_{+-}$ CT descriptors for $T_1$, $T_2$ and $S_1$ excited states. Apart from **DACT-II**, the nature of the $S_1$ state is in good agreement with SCS-CC2 when considering the CAM-B3LYP and the M06-2X functionals for both TD-DFT or TDA-DFT calculations. By contrast, B3LYP and PBE0 perform the worst with $S_1$ states predicted to have a larger CT character. When tuning the range separation parameter, LC-ω*PBE and LC-ω*HPBE perform better compared to the original LC-ωPBE functional and with a similar accuracy as for the CAM-B3LYP and M06-2X functionals. Overall, we found that regardless of the functional the excited state description is not as well reproduced for triplets as it is for singlets, which is reflected in the larger MAD for

every CT descriptor. Of the functionals assessed that did not require parameter tuning, both CAM-B3LYP and M06-2X provide the most accurate predictions of the character of the low-lying excited states. We therefore encourage the community to adopt either of these two functionals in combination with TDA-DFT calculations in order to obtain the most accurate modelling for TADF materials, however direct assignment of $T_1$ and $T_2$ natures must be done with caution.

## Supporting Information

Photophysical and device data of studied emitters and supplementary computational data of all studied emitters along with coordinates.

## Acknowledgments

The St Andrews team would like to thank the Leverhulme Trust (RPG-2016-047) for financial support. Computational resources have been provided by the Consortium des Équipements de Calcul Intensif (CÉCI), funded by the Fonds de la Recherche Scientifiques de Belgique (F.R.S.-FNRS) under Grant No. 2.5020.11, as well as the Tier-1 supercomputer of the Fédération Wallonie-Bruxelles, infrastructure funded by the Walloon Region under the grant agreement n1117545. Y.O. acknowledges funding by the Fonds de la Recherche Scientifique-FNRS under Grant n° F.4534.21 (MIS-IMAGINE). D.B. is a FNRS Research Director.

## References

1. Y. Liu, C. Li, Z. Ren, S. Yan and M. R. Bryce, *Nat. Rev. Mater.,* 2018, **3**, 18020.
2. Y. Tao, K. Yuan, T. Chen, P. Xu, H. Li, R. Chen, C. Zheng, L. Zhang and W. Huang, *Adv. Mater.,* 2014, **26**, 7931.
3. T. J. Penfold, F. B. Dias and A. P. Monkman, *Chem. Commun.,* 2018, **54**, 3926.
4. M. Y. Wong and E. Zysman-Colman, *Adv. Mater.,* 2017, **29**, 1605444.
5. A. Maciejewski, M. Szymanski and R. P. Steer, *J. Phys. Chem.,* 1986, **90**, 6314.

6. M. W. Wolf, K. D. Legg, R. E. Brown, L. A. Singer and J. H. Parks, *J. Am. Chem. Soc.,* 1975, **97**, 4490.
7. C. A. Parker and C. G. Hatchard, *Trans. Faraday Soc.,* 1961, **57**, 1894.
8. F. A.Salazar, A. Fedorov and M. N.Berberan-Santos, *Chem. Phys. Lett.,* 1997, **271**, 361.
9. H. Uoyama, K. Goushi, K. Shizu, H. Nomura and C. Adachi, *Nature,* 2012, **492**, 234.
10. J. C. Deaton, S. C. Switalski, D. Y. Kondakov, R. H. Young, T. D. Pawlik, D. J. Giesen, S. B. Harkins, A. J. M. Miller, S. F. Mickenberg and J. C. Peters, *J. Am. Chem. Soc.,* 2010, **132**, 9499.
11. C. M. Marian, *WIREs Computational Molecular Science,* 2012, **2**, 187.
12. S. K. Lower and M. A. El-Sayed, *Chem. Rev.,* 1966, **66**, 199.
13. A. Köhler and H. Bässler, *Mater. Sci. Eng., R,* 2009, **66**, 71.
14. J. Gibson, A. P. Monkman and T. J. Penfold, *ChemPhysChem,* 2016, **17**, 2956.
15. N. Aizawa, A. Matsumoto and T. Yasuda, *Sci. Adv.,* 2021, **7**, eabe5769.
16. P. L. dos Santos, J. S. Ward, D. G. Congrave, A. S. Batsanov, J. Eng, J. E. Stacey, T. J. Penfold, A. P. Monkman and M. R. Bryce, *Adv. Sci.,* 2018, **5**, 1700989.
17. H. Noda, X.-K. Chen, H. Nakanotani, T. Hosokai, M. Miyajima, N. Notsuka, Y. Kashima, J.-L. Brédas and C. Adachi, *Nat. Mater.,* 2019, **18**, 1084.
18. L.-S. Cui, A. J. Gillett, S.-F. Zhang, H. Ye, Y. Liu, X.-K. Chen, Z.-S. Lin, E. W. Evans, W. K. Myers, T. K. Ronson, H. Nakanotani, S. Reineke, J.-L. Bredas, C. Adachi and R. H. Friend, *Nat. Photonics,* 2020, **14**, 636.
19. Y. Wada, H. Nakagawa, S. Matsumoto, Y. Wakisaka and H. Kaji, *Nat. Photonics,* 2020, **14**, 643.
20. Y. Olivier, B. Yurash, L. Muccioli, G. D'Avino, O. Mikhnenko, J. C. Sancho-García, C. Adachi, T. Q. Nguyen and D. Beljonne, *Phys. Rev. Mater.,* 2017, **1**, 075602.
21. A. D. Laurent and D. Jacquemin, *Int. J. Quantum Chem.,* 2013, **113**, 2019.
22. S. Hirata and M. Head-Gordon, *Chem. Phys. Lett.,* 1999, **314**, 291.
23. M. Moral, L. Muccioli, W. J. Son, Y. Olivier and J. C. Sancho-García, *J. Chem. Theory Comput.,* 2015, **11**, 168.
24. T. J. Penfold, *J. Phys. Chem. C,* 2015, **119**, 13535.
25. H. Sun, C. Zhong and J.-L. Brédas, *J. Chem. Theory Comput.,* 2015, **11**, 3851.
26. Y. Shu and B. G. Levine, *J. Chem. Phys.,* 2015, **142**, 104104.
27. R. Gómez-Bombarelli, J. Aguilera-Iparraguirre, T. D. Hirzel, D. Duvenaud, D. Maclaurin, M. A. Blood-Forsythe, H. S. Chae, M. Einzinger, D. G. Ha, T. Wu, G. Markopoulos, S. Jeon, H. Kang, H. Miyazaki, M. Numata, S. Kim, W. Huang, S. I. Hong, M. Baldo, R. P. Adams and A. Aspuru-Guzik, *Nat. Mater.,* 2016, **15**, 1120.
28. A. D. Becke, *J. Chem. Phys.,* 1993, **98**, 5648.
29. C. Adamo and V. Barone, *J. Chem. Phys.,* 1999, **110**, 6158.
30. D. Jacquemin, E. A. Perpète, I. Ciofini and C. Adamo, *Theor. Chem. Acc.,* 2010, **128**, 127.
31. J.-D. Chai and M. Head-Gordon, *Phys. Chem. Chem. Phys.,* 2008, **10**, 6615.
32. O. A. Vydrov and G. E. Scuseria, *J. Chem. Phys.,* 2006, **125**, 234109.
33. J. Eng, B. A. Laidlaw and T. J. Penfold, *J. Comput. Chem.,* 2019, **40**, 2191.
34. Y. Zhao and D. G. Truhlar, *Theor. Chem. Acc.,* 2008, **120**, 215.
35. J. Sanz-Rodrigo, Y. Olivier and J. C. Sancho-Garcia, *Molecules,* 2020, **25**, 1006.
36. S. Grimme, L. Goerigk and R. F. Fink, *Wiley Interdiscip. Rev. Comput. Mol. Sci.,* 2012, **2**, 886.
37. C. Brückner and B. Engels, *Chem. Phys.,* 2017, **482**, 319.
38. A. Pershin, D. Hall, V. Lemaur, J.-C. Sancho-Garcia, L. Muccioli, E. Zysman-Colman, D. Beljonne and Y. Olivier, *Nat. Commun.,* 2019, **10**, 597.
39. T. Northey, J. Stacey and T. J. Penfold, *J. Mater. Chem. C.,* 2017, **5**, 11001.
40. T. Hu, G. Han, Z. Tu, R. Duan and Y. Yi, *J. Phys. Chem. C,* 2018, **122**, 27191.
41. L. Kunze, A. Hansen, S. Grimme and J.-M. Mewes, *J. Phys. Chem. Lett.,* 2021, 8470.
42. T. Cardeynaels, S. Paredis, J. Deckers, S. Brebels, D. Vanderzande, W. Maes and B. Champagne, *Phys. Chem. Chem. Phys.,* 2020, **22**, 16387.

43. M. K. Etherington, J. Gibson, H. F. Higginbotham, T. J. Penfold and A. P. Monkman, *Nat. Commun.,* 2016, **7**, 13680.
44. F. B. Dias, T. J. Penfold and A. P. Monkman, *Methods Appl. Fluoresc.,* 2017, **5**, 012001.
45. X.-K. Chen, Y. Tsuchiya, Y. Ishikawa, C. Zhong, C. Adachi and J.-L. Brédas, *Adv. Mater.,* 2017, **29**, 1702767.
46. Y. Olivier, J. C. Sancho-Garcia, L. Muccioli, G. D'Avino and D. Beljonne, *J. Phys. Chem. Lett.,* 2018, **9**, 6149.
47. A. Dreuw and M. Head-Gordon, *Chem. Rev.,* 2005, **105**, 4009.
48. C. A. Guido, P. Cortona and C. Adamo, *J. Chem. Phys.,* 2014, **140**, 104101.
49. M. Savarese, C. A. Guido, E. Brémond, I. Ciofini and C. Adamo, *J. Phys. Chem. A.,* 2017, **121**, 7543.
50. T. Yanai, D. P. Tew and N. C. Handy, *Chem. Phys. Lett.,* 2004, **393**, 51.
51. M. A. Rohrdanz, K. M. Martins and J. M. Herbert, *J. Chem. Phys.,* 2009, **130**, 054112.
52. S. Grimme, J. Antony, S. Ehrlich and H. Krieg, *J. Chem. Phys.,* 2010, **132**, 154104.
53. G. A. Petersson and M. A. Al-Laham, *J. Chem. Phys.,* 1991, **94**, 6081.
54. C. Hättig and F. Weigend, *J. Chem. Phys.,* 2000, **113**, 5154.
55. C. Hättig and K. Hald, *Phys. Chem. Chem. Phys.,* 2002, **4**, 2111.
56. A. Tajti and P. G. Szalay, *J. Chem. Theory Comput.,* 2019, **15**, 5523.
57. J. Thorn H. Dunning, *J. Chem. Phys.,* 1989, **90**, 1007.
58. T. Helgaker, S. Coriani, P. Jorgensen, K. Kristensen, J. Olsen and K. Ruud, *Chem. Rev.,* 2012, **112**, 543.
59. M. J. Frisch, G. W. Trucks, H. B. Schlegel, G. E. Scuseria, M. A. Robb, J. R. Cheeseman, G. Scalmani, V. Barone, B. Mennucci, G. A. Petersson, H. Nakatsuji, M. Caricato, X. Li, H. P. Hratchian, A. F. Izmaylov, J. Bloino, G. Zheng, J. L. Sonnenberg, M. Hada, M. Ehara, K. Toyota, R. Fukuda, J. Hasegawa, M. Ishida, T. Nakajima, Y. Honda, O. Kitao, H. Nakai, T. Vreven, J. A. M. Jr., J. E. Peralta, F. Ogliaro, M. Bearpark, J. J. Heyd, E. Brothers, K. N. Kudin, V. N. Staroverov, R. Kobayashi, J. Normand, K. Raghavachari, A. Rendell, J. C. Burant, S. S. Iyengar, J. Tomasi, M. Cossi, N. Rega, J. M. Millam, M. Klene, J. E. Knox, J. B. Cross, V. Bakken, C. Adamo, J. Jaramillo, R. Gomperts, R. E. Stratmann, O. Yazyev, A. J. Austin, R. Cammi, C. Pomelli, J. W. Ochterski, R. L. Martin, K. Morokuma, V. G. Zakrzewski, G. A. Voth, P. Salvador, J. J. Dannenberg, S. Dapprich, A. D. Daniels, Ö. Farkas, J. B. Foresman, J. V. Ortiz, J. Cioslowski and D. J. Fox *Gaussian 09*, Gaussian Inc., Wallingford, CT: 2009.
60. M. J. Frisch, G. W. Trucks, H. B. Schlegel, G. E. Scuseria, M. A. Robb, J. R. Cheeseman, G. Scalmani, V. Barone, G. A. Petersson, H. Nakatsuji, X. Li, M. Caricato, A. V. Marenich, J. Bloino, B. G. Janesko, R. Gomperts, B. Mennucci, H. P. Hratchian, J. V. Ortiz, A. F. Izmaylov, J. L. Sonnenberg, Williams, F. Ding, F. Lipparini, F. Egidi, J. Goings, B. Peng, A. Petrone, T. Henderson, D. Ranasinghe, V. G. Zakrzewski, J. Gao, N. Rega, G. Zheng, W. Liang, M. Hada, M. Ehara, K. Toyota, R. Fukuda, J. Hasegawa, M. Ishida, T. Nakajima, Y. Honda, O. Kitao, H. Nakai, T. Vreven, K. Throssell, J. A. Montgomery Jr., J. E. Peralta, F. Ogliaro, M. J. Bearpark, J. J. Heyd, E. N. Brothers, K. N. Kudin, V. N. Staroverov, T. A. Keith, R. Kobayashi, J. Normand, K. Raghavachari, A. P. Rendell, J. C. Burant, S. S. Iyengar, J. Tomasi, M. Cossi, J. M. Millam, M. Klene, C. Adamo, R. Cammi, J. W. Ochterski, R. L. Martin, K. Morokuma, O. Farkas, J. B. Foresman and D. J. Fox *Gaussian 16 Rev. A.01*, Wallingford, CT, 2016.
61. *TURBOMOLE V7.4*, TURBOMOLE GmbH, since 2007; avaliable from http://www.turbomole.com: a development of University of Karlsruhe and Forschungszentrum Karlsruhe GmbH, 2017.
62. J. Eng, J. Hagon and T. J. Penfold, *J. Mater. Chem. C.,* 2019, **7**, 12942.
63. E. Zysman-Colman, *Nat. Photonics,* 2020, **14**, 593.
64. T. Etienne, X. Assfeld and A. Monari, *J. Chem. Theory Comput.,* 2014, **10**, 3896.
65. T. Etienne, X. Assfeld and A. Monari, *J. Chem. Theory Comput.,* 2014, **10**, 3906.
66. T. Lu and F. Chen, *J. Comput. Chem.,* 2012, **33**, 580.
67. T. Le Bahers, C. Adamo and I. Ciofini, *J. Chem. Theory Comput.,* 2011, **7**, 2498.

68. L. Huet, A. Perfetto, F. Muniz-Miranda, M. Campetella, C. Adamo and I. Ciofini, *J. Chem. Theory Comput.,* 2020, **16**, 4543.
69. *n=13 for calculation of MAD data from nature, owing to DACT-II being identified as an outlier.*
.

TOC

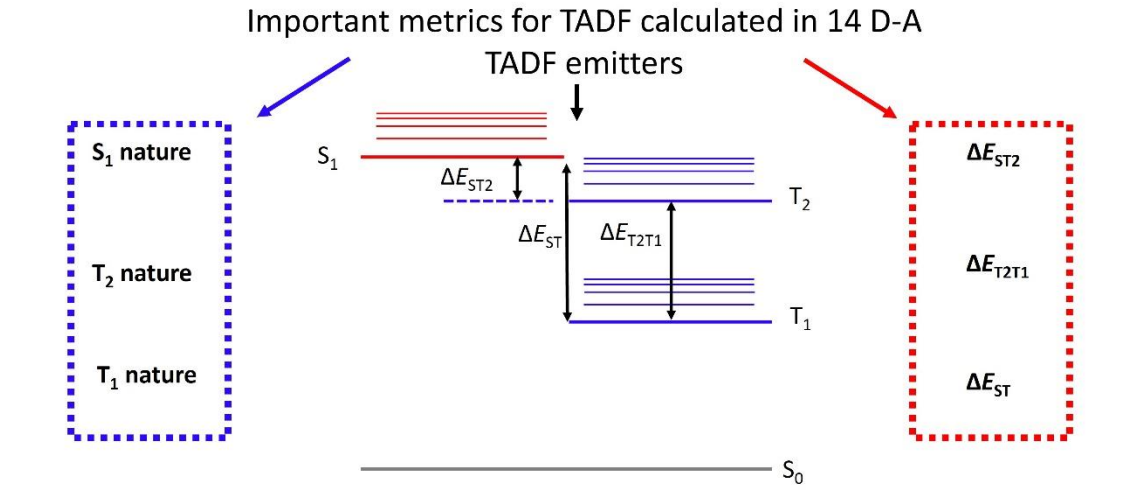


SCS-CC2 vs B3LYP, PBE0, M06-2X, LC-ωPBE, LC-ω*PBE, LC-ω*HPBE & CAM-B3LYP

**M06-2X and CAM-B3LYP offer most consistent results!**